



## ORIGINAL ARTICLE

# The effect of polyoxyethylene (40) stearate surfactant on novel synthesis of mesoporous $\gamma$ -alumina from Kano kaolin



Abdul Rahim Yacob <sup>a</sup>, Abdu Muhammad Bello <sup>a,b,\*</sup>,  
Kamaluddeen Suleiman Kabo <sup>a,b</sup>

<sup>a</sup> Department of Chemistry, Faculty of Science, University of Technology Malaysia, UTM Skudai, 81310 Johor, Malaysia

<sup>b</sup> Department of Chemistry, School of Natural and Applied Sciences, Sa'adatu Rimi College of Education Kumbotso, PMB 3218, Kano State, Nigeria

Received 2 December 2014; accepted 30 June 2015

Available online 8 July 2015

## KEYWORDS

Kano kaolin;  
Mesoporous  $\gamma$ -alumina;  
Polyoxyethylene (40) stearate (PS);  
Surfactant

**Abstract** Mesoporous  $\gamma$ -alumina was synthesized by acid extraction of alumina from Kano kaolin using polyoxyethylene (40) stearate (PS) as a surfactant. The synthesized alumina was characterized using X-ray diffraction (XRD),  $N_2$  adsorption–desorption, Fourier transform infra-red spectroscopy (FTIR), field emission scanning electron microscopy attached with energy-dispersive X-ray (FESEM–EDX), and thermogravimetric analysis (TG–DTA). High-purity mesoporous  $\gamma$ - $Al_2O_3$  with relatively large surface area and narrow pore size distribution was obtained. For comparison the preparation in the absence of surfactant was also carried out. In this study mesoporous alumina was also obtained even in the absence of the surfactant, however, the addition of PS resulted in modification on physical properties and morphology. The surface area increased from 169.0  $m^2/g$  to 222.7  $m^2/g$ , pore size from 4.4 nm to 5.6 nm and pore volume from 0.32  $cm^3/g$  to 0.45  $cm^3/g$ . Crystallite size was also found to increase from 2.68 nm to 3.33 nm after the addition of the surfactant.

© 2015 The Authors. Production and hosting by Elsevier B.V. on behalf of King Saud University. This is an open access article under the CC BY-NC-ND license (<http://creativecommons.org/licenses/by-nc-nd/4.0/>).

## 1. Introduction

The discovery of M41S type molecular sieves by Mobil Oil Corp in 1990 has open the door for material scientist for synthesis of silica and alumina based mesoporous materials (Ghosh et al., 2015). Mesoporous alumina (Jiang et al., 2012), titania (Oveisi et al., 2010) and zirconia were the first few materials to be synthesized. The synthesis of mesoporous alumina however is not direct as compared to silicates in the M41S family. Different chemical behaviour of

\* Corresponding author at: Department of Chemistry, Faculty of Science, University of Technology Malaysia, UTM Skudai, 81310 Johor, Malaysia. Tel.: +60 149142616.

E-mail address: [muhbaf70@yahoo.com](mailto:muhbaf70@yahoo.com) (A.M. Bello).

Peer review under responsibility of King Saud University.



Production and hosting by Elsevier

alumina leads to the failure of the synthesis in organized mesoporous alumina. By the end of twentieth century, organized mesoporous aluminas was synthesized following several modifications of the procedures for silica materials (Márquez-Alvarez et al., 2008). Alumina exists in various meta-stable states including the  $\gamma$ -,  $\eta$ -,  $\sigma$ -,  $\theta$ -,  $\kappa$ - and  $\chi$ -phase, and the stable  $\alpha$ -  $\text{Al}_2\text{O}_3$  phase (Yang et al., 2010). Due to its physical, textural, thermal, and chemical properties, mesoporous  $\gamma$ -alumina is the most extensively used in a wide range of catalytic processes, separation process, host guest chemistry, adsorbents host for quantum structures, separation of large biological molecules, and environmental pollution control. The pore structural properties of mesoporous  $\gamma$ -alumina, high surface area and large pore volume, allow for higher loading of active catalytic phases.

The synthesis of mesoporous alumina has been reported through various chemical routes viz.: hydrolysis (Jiao et al., 2012; Khalil, 2008), sol-gel (Awual and Hasan, 2014; Sapniwat et al., 2013; Feng et al., 2011), hydrothermal process (Shi et al., 2014; Yue et al., 2011 and Zhu et al., 2009b) in the presence of aluminium salts, alkoxides and metal powders as precursor. The mentioned precursors are however, expensive and corrosive making the preparation both unsafe and uneconomical.

Kaolin is an abundant, cheap and environmentally friendly mineral as compared to the aluminium alkoxides or inorganic salts as precursor for the synthesis of mesoporous  $\gamma$ - $\text{Al}_2\text{O}_3$ . Alumina can be synthesized from kaolin by either direct conversion of kaolin into  $\gamma$ -alumina using concentrated base solution, or by extraction of the alumina phase from the kaolin crystal structure with acidic solution (Samadhi et al., 2011). Several authors have described the synthesis of alumina from kaolin; Du and Yang (2012) reported the synthesis of aluminium containing hexagonal ordered mesoporous silica Al-MCM-41 through hydrothermal treatment of leached products produced by pre-grinding and subsequent acid leaching of natural kaolin, without the addition of silica or aluminium reagents. Pan et al. (2013) synthesized mesoporous  $\gamma$ - $\text{Al}_2\text{O}_3$  from coal-series kaolin in the presence of cetyltrimethylammonium bromide (CTAB). Synthesis of mesoporous  $\gamma$ -alumina from kaolin using precipitation method in the presence of ammonia and PEG-4500 as surfactant was reported by Darban et al. (2013).

In this study polyoxyethylene (40) stearate (PS) was used for the first time in the synthesis of high-purity mesoporous alumina from Kano kaolin. PS is a non-ionic surfactant and is considered not hazardous according to OSHA Hazard Communication Standard (HCS) under the toxic and hazardous substances (29 CFR 1910.1200). This will allow for an environmentally benign synthesis of alumina as both the surfactant and kaolin are non-toxic. PS is used as emulsifier and solubilizer, and due to its non-toxic nature is also used in pharmacy as carrier of solid dispersion to improve the dissolution of griseofulvin and also as excipient (Zhu et al., 2009a). The study is aimed at investigating the effect of PS on the synthesis of mesoporous alumina as compared in the absence of the surfactant. To the best of our knowledge there was no report on the synthesis of mesoporous alumina in the presence of this surfactant.

## 2. Experimental

### 2.1. Materials

The kaolin was obtained from Getso town in Kano state, Nigeria. Henceforth the kaolin will be known as Kano kaolin. Hydrochloric acid and sodium hydroxide were obtained from QR $\text{\textcircled{R}}$ C $^{\text{TM}}$ , while polyoxyethylene (40) stearate [poly(oxy-1,2-ethanediyl), alpha-hydro-omega-hydroxy-, octadecanoate] was obtained from Sigma. All the reagents were of analytical grade and used without further purification. The polyoxyethylene (40) stearate henceforth will be referred to as PS.

### 2.2. Synthesis of mesoporous alumina

The Kano kaolin was calcined into metakaolin in a programmable furnace at 750 °C for 3 h with heating rate of 5 °C/min. The metakaolin was leached with 6 M hydrochloric acid at 90 °C for 2.5 h under stirring at 836 rpm (solid/liquid ratio 1:5 g/mL), the suspension was filtered followed by the addition of excess solution of 5 M NaOH, alumina was converted into  $\text{NaAlO}_2$  and impurities such as  $\text{Fe}^{3+}$ ,  $\text{Mg}^{2+}$  presence were precipitated. After filtration 6 M HCl was added to the  $\text{NaAlO}_2$  solution with stirring to adjust the pH to 7, and the precipitate formed was filtered and washed with deionized water. The solid obtained was mixed vigorously with a solution of PS containing 1.8 g in 100 mL of water for 19 h, and the suspension aged for 2 days at room temperature. It was then filtered, washed with deionized water, dried at 120 °C, followed by calcination at 500 °C for 4 h. The obtained alumina is named  $\text{Al}_2\text{O}_3$ -PS-500. Another alumina was prepared using the same procedure but without the addition of surfactant and is denoted as  $\text{Al}_2\text{O}_3$ -500. The PS concentration was above the critical micelle concentration (CMC) which was reported to be  $>97.8 \mu\text{M}$  (Zhu et al., 2009a).

#### 2.2.1. Characterization

The ignition loss was determined by calcination of the kaolin sample at 600 °C for 3 h. The chemical composition was determined using energy dispersive X-ray fluorescence spectrometer NEXCG (USA). Structural phase analysis was carried out on a Bruker D8 having Siemens Diffractometer D5000 with Cu K $\alpha$  radiation (40 kV, 40 mA,  $\lambda = 1.5406 \text{ \AA}$ ) (USA). The morphology and the chemical composition of the samples were obtained by field emission electron microscopy/energy dispersive X-ray analysis (FESEM-EDX) (Supra $^{\text{TM}}$  35 VP operating at 10 kV) (Germany). The TG-DTA analysis was carried out using Perkin Elmer Simultaneous Thermal Analyzer (STA 8000) (USA) in the temperature range of 50–1200 °C at heating rate of 10 °C/min.  $\text{N}_2$  adsorption-desorption was used to determine the surface area, pore size distribution and pore volume at  $-196 \text{ }^\circ\text{C}$  using Fisher Thermo Scientific SURFER (USA), prior to analysis all samples were dehydrated and degassed by evacuation at 300 °C for 3 h. Perkin Elmer 1650 Infra-Red Spectrometer (USA) was used for FTIR analysis of samples in the range of 4000–400  $\text{cm}^{-1}$ .

### 3. Results and discussion

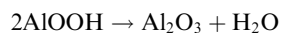
#### 3.1. Chemical composition

The XRF analysis was carried out to estimate the chemical composition of the kaolin and that of mesoporous alumina. The kaolin consists mainly of silica and alumina, with other metal oxides such as  $\text{Fe}_2\text{O}_3$  and  $\text{MnO}_2$  occurring as minor. The percentage composition by mass of the elements present in the kaolin sample was found to be as follows:  $\text{SiO}_2$ , 58.2;  $\text{Al}_2\text{O}_3$ , 39.2;  $\text{Fe}_2\text{O}_3$ , 1.44;  $\text{K}_2\text{O}$ , 0.841;  $\text{MnO}_2$ , 0.0679;  $\text{TiO}_2$ , 0.0589;  $\text{CaO}$ , 0.0525 and ignition loss, 13.13%. The loss on ignition may be a result of organic matter lost and/or some non-metals like sulphur which could have been removed in the form of  $\text{SO}_2$  (Eze et al., 2012; Mohsen and El-maghraby, 2010). The Kano kaolin has high content of aluminium making it a good candidate for synthesis of alumina. The composition of  $\text{Al}_2\text{O}_3$  in the mesoporous gamma alumina was found to be 98% indicating very high purity of the synthesized alumina and demonstrating the advantage of using the procedure for the synthesis of pure alumina from kaolin.

#### 3.2. TG-DTA analysis

From the TGA curve of the boehmite precursor synthesized in the presence of PS presented in Fig. 1, two major weight losses can be observed; the first one is around 13.3% that occurred in the region between 50 and 190 °C corresponding to an endothermic peak at 89.43 °C in the DTA curve, this can be attributed to the desorption of physically adsorbed water and removal of template, as the boiling point of PS is above 100 °C. The second mass loss amounting to 17.9% took place between 230 and 590 °C equivalent to the second endothermic peak at 354.4 °C in the DTA curve could be due to the release of chemically adsorbed water molecules leading to the conversion of  $\text{AlOOH}$  to  $\text{Al}_2\text{O}_3$ . For the precursor synthesized without surfactant, two mass losses were also observed, the first mass loss due to the removal of physically adsorbed water is 11.8% and the second one is 18.0%. The observed decrease in the weight loss due to the removal of physically adsorbed water for the precursor synthesized in the absence of surfactant

compared with the one in the presence of PS confirmed the assumption that the first mass loss in the later is due to both removal of physically adsorbed water plus template. Above 600 °C the weight loss process stabilized, this indicates the beginning of various alumina phase transformation, and it also suggest good thermal stability of the synthesized  $\gamma\text{-Al}_2\text{O}_3$ . The exothermic peak around 500 °C will be assigned to the initial formation of  $\gamma\text{-Al}_2\text{O}_3$  by dehydroxylation of boehmite (Khalil, 2008). From the dehydroxylation reaction of boehmite shown below:



The expected weight loss would be about 15% against 35% in the case of aluminium hydroxide. The agreement between the observed weight loss and the stoichiometric value strongly supports that the precursor is aluminium oxyhydroxide not aluminium hydroxide.

The differential scanning calorimetry DSC presented in Fig. 2 concurs with the TG-DTA result. Three endothermic peaks can be observed for the precursor synthesized with PS at 91.55, 365.67 and 656.28 °C, respectively. The first peak could be attributed to desorption of physically adsorbed water molecules, the second due to the release of chemically desorbed water molecules and decomposition and/or combustion of the surfactant template and the last may be associated with the phase transition process of the alumina (Rangel-Porras et al., 2015; Zhu et al., 2009b).

#### 3.3. XRD analysis

The wide-angle X-ray diffraction pattern presented in Fig. 3, depicts the spectra obtained for the precursor,  $\text{Al}_2\text{O}_3\text{-PS-500}$  and  $\text{Al}_2\text{O}_3\text{-500}$ . The characteristic diffraction peaks of the precursor are those of Al(hydr)oxide ( $\text{AlOOH}$ ) (JCPDS Card no. 21-1307) that points to the orthorhombic structure of the precursor, and five diffraction peaks were observed at  $2\theta = 12^\circ$ ,  $28^\circ$ ,  $38^\circ$ ,  $49^\circ$  and  $65^\circ$  corresponding to [020], [120], [031], [200] and [002] crystal planes respectively. This finding corroborates the assertion from the TG-DTA result that the precursor is aluminium oxyhydroxide.

The calcined samples showed characteristic peaks at  $2\theta = 32^\circ$ ,  $38^\circ$ ,  $46^\circ$ , and  $67^\circ$  that correspond respectively to

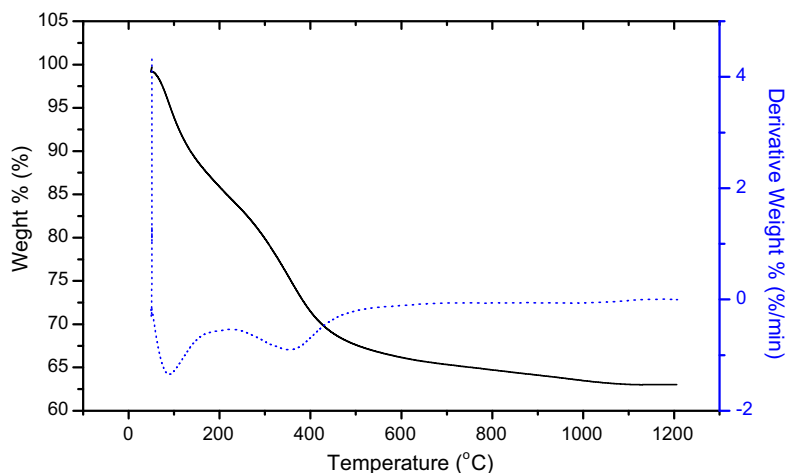
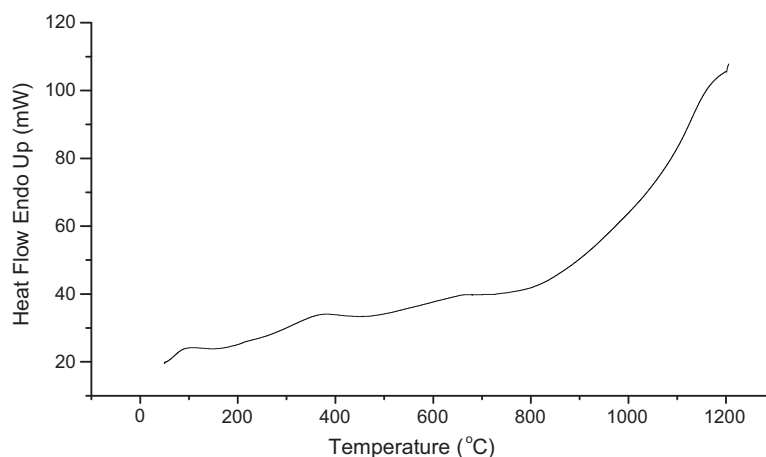
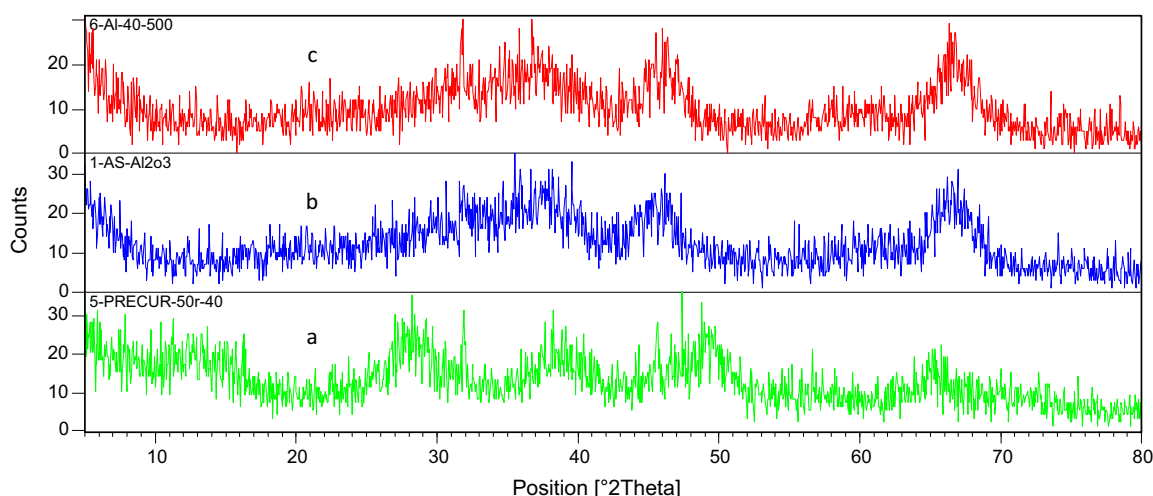


Figure 1 TG-DTA curve of the precursor with PS.



**Figure 2** DSC curve of the precursor synthesized with PS.



**Figure 3** XRD pattern of; (a) precursor, (b)  $\text{Al}_2\text{O}_3$ -500 and (c)  $\text{Al}_2\text{O}_3$ -PS-500.

[220], [311], [400] and [440] crystal planes (JCPDS Card no 10-0425) which is that of a face-centred cubic lattice. The absence of [002] peak, which is characteristic of boehmite indicates the formation of  $\gamma$ -alumina. The broadening of the XRD peaks clearly indicates the mesoporous nature of the crystallites (Afruz and Tafreshi, 2014).

The crystallite size of the alumina was calculated using Scherer's formula from the three most intense peaks:  $38^\circ$ ,  $46^\circ$  and  $67^\circ$  and the results obtained are 3.04, 3.31 and 3.62 nm with an average of 3.33 nm for  $\text{Al}_2\text{O}_3$ -PS-500 and 1.76, 3.11 and 3.18 nm with an average of 2.68 nm for  $\text{Al}_2\text{O}_3$ -500. The result indicates that the addition of the surfactant resulted in an increase of the crystallite size, as well as making it more regular. For the precursor the average crystallite size was found to be 3.21 nm.

#### 3.4. FTIR analysis

The FTIR spectra of the precursor,  $\text{Al}_2\text{O}_3$ -PS-500 and  $\text{Al}_2\text{O}_3$ -500 are presented in Fig. 4. All samples showed broad bands around  $3480\text{ cm}^{-1}$  assigned to the stretching vibration of structural OH attached to  $\text{Al}_2\text{O}_3$  indicating the presence of

molecular water and around  $1635\text{ cm}^{-1}$  due to  $\delta\text{OH}$  bending vibration mode of adsorbed water (Xue et al., 2009). The band around  $1075\text{ cm}^{-1}$  is attributed to symmetrical Al-OH bending modes which confirmed the formation of boehmite (Liu et al., 2008; Yang et al., 2010). Band around  $1386\text{ cm}^{-1}$  is caused by adsorbed non-structural  $\text{CO}_3^{2-}$  during sample preparation process (Zhu et al., 2009b).

Bands around  $945$  and  $498\text{ cm}^{-1}$  can be assigned to C-O-C and  $-\text{CH}_2-$  vibration that originates from the surfactant, and their absence after calcination indicates that the alumina is free from surfactant. The band around  $785\text{ cm}^{-1}$  is attributed to the stretching mode of  $\text{AlO}_4$  (tetrahedral Al-O) and that around  $590\text{ cm}^{-1}$  is associated with stretching vibration mode of  $\text{AlO}_6$  (octahedral Al-O). The formation of alumina is confirmed by absence of band around  $1075\text{ cm}^{-1}$  (Pan et al., 2013; Yang et al., 2010).

#### 3.5. Porosity measurement

The  $\text{N}_2$  adsorption-desorption isotherm of the aluminas are presented in Figs. 5 and 6, while pore size distribution curve presented in Figs. 7 and 8. Both samples showed type IV

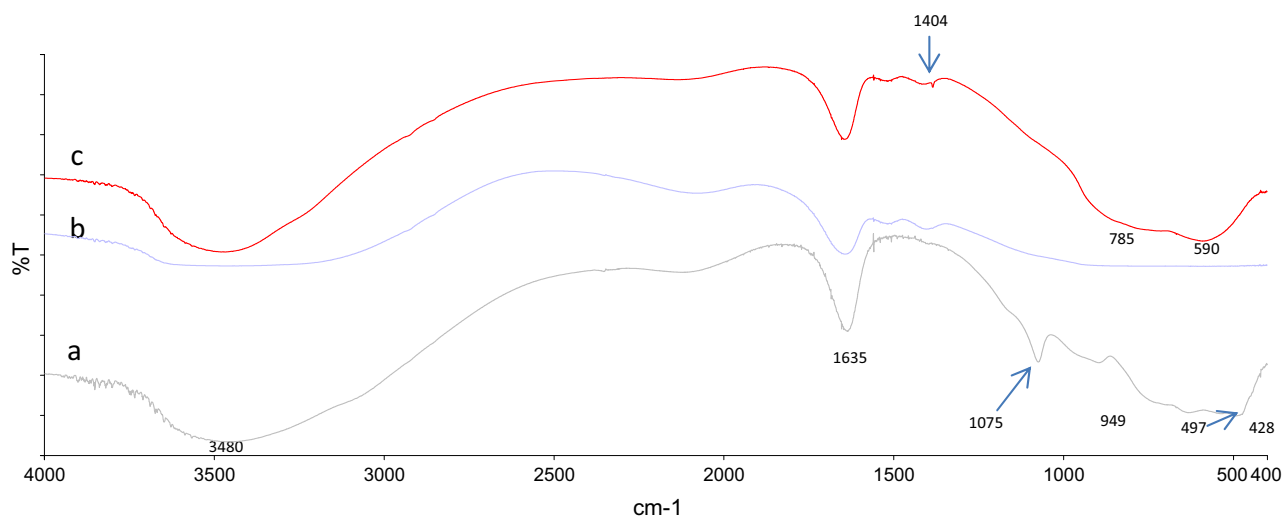


Figure 4 FTIR spectra of; (a) precursor, (b)  $\text{Al}_2\text{O}_3$ -500 and (c)  $\text{Al}_2\text{O}_3$ -PS-500.

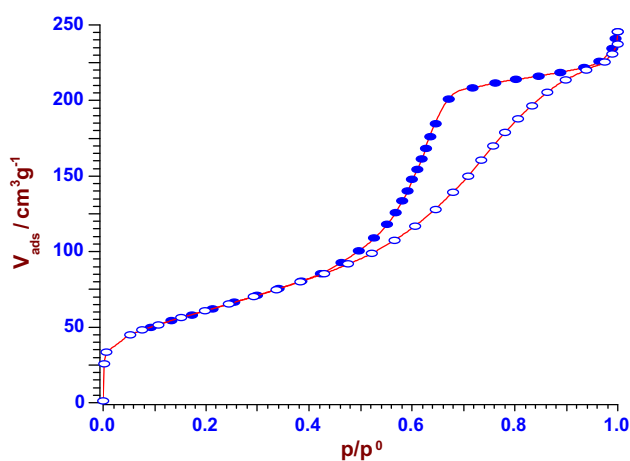


Figure 5  $\text{N}_2$ -adsorption-desorption isotherm of  $\text{Al}_2\text{O}_3$ -PS-500.

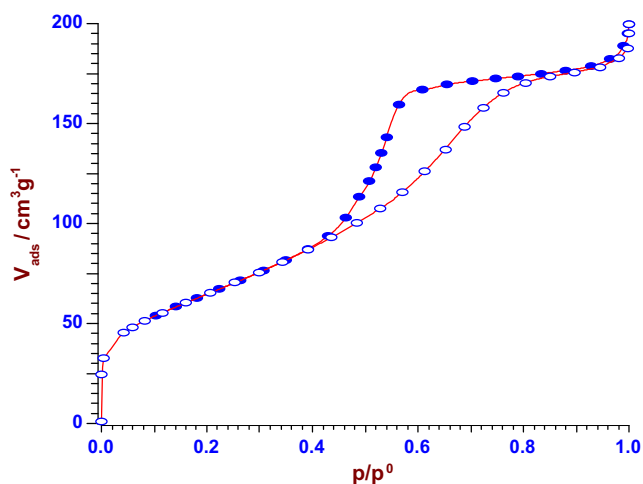


Figure 6  $\text{N}_2$ -adsorption-desorption isotherm of  $\text{Al}_2\text{O}_3$ -500.

isotherm with H2 hysteresis loops at high pressure indicating the existence of mesoporous materials. Similar observation was made by other researchers for the synthesis of mesoporous alumina without surfactant, this was attributed to inter particles pores formed by the close stacking of primary and secondary particles, and the formation of inter particle pores cannot be controlled since it only depends on the shape, the uniformity and the arrangement of the primary and secondary particles in the precursor (Lesaint et al., 2009; Liu et al., 2006).

Type H2 hysteresis loop usually results from closely packed spherical particles with uniform size or from complex, interconnected pore network. The H2 hysteresis observed for the sample indicates relatively non-uniform pores are present in the alumina, consistent with the isotherm which shows both microporous and mesoporous structures. The observed step increase at low  $P/P_0$  is probably due to monolayer adsorption and additional micro-porosity of the sample which further supports the observation from BJH analysis (Polarz, 2004). The adsorption and desorption branches of the hysteresis loop do not close until  $P/P_0$  approaches 0.8–0.9 indicating that the pores are formed by the interstices between plate-like aggregates. The broad hysteresis loop centring at higher  $P/P_0$  is an indication of larger mesopores (Jiao et al., 2012).

The pore size distribution of  $\text{Al}_2\text{O}_3$ -PS-500 and  $\text{Al}_2\text{O}_3$ -500 showed narrow distributions centred at 5.6 nm and 4.4 nm and pore volumes of  $0.45 \text{ cm}^3/\text{g}$  and  $0.32 \text{ cm}^3/\text{g}$ , respectively. According to IUPAC classification, mesoporous solids contain pores with pore diameter between 2 and 50 nm (Naik and Ghosh 2009). The steeper curve in the capillary condensation initiated the narrow pore size distribution and the saturation of the isotherms at large relative vapour pressure values caused the observed limiting porous volume (Kang et al., 2004).

From the BET result, the surface area of the  $\text{Al}_2\text{O}_3$ -PS-500 was found to be  $222.7 \text{ m}^2/\text{g}$  and that of  $\text{Al}_2\text{O}_3$ -500 is  $169.0 \text{ m}^2/\text{g}$ . Although mesoporous alumina is formed even in the absence of surfactant, its addition played an important role in obtaining mesoporous alumina with large surface area and distribution centred at higher relative pressure (Lesaint et al., 2009). Enhancement of catalytic activity can be contributed by large surface area, narrow pore-size and excellent thermal stability (Zhu et al., 2009b).

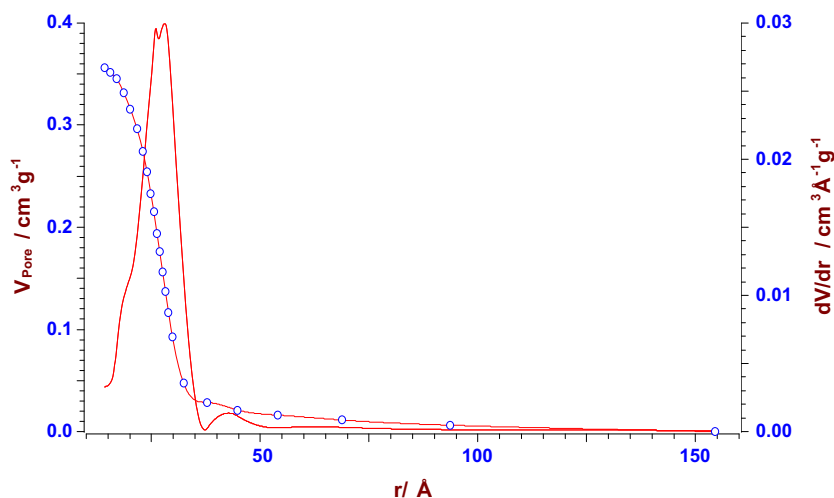


Figure 7 Pore distribution (B.J.H.) of  $\text{Al}_2\text{O}_3\text{-PS-500}$ .

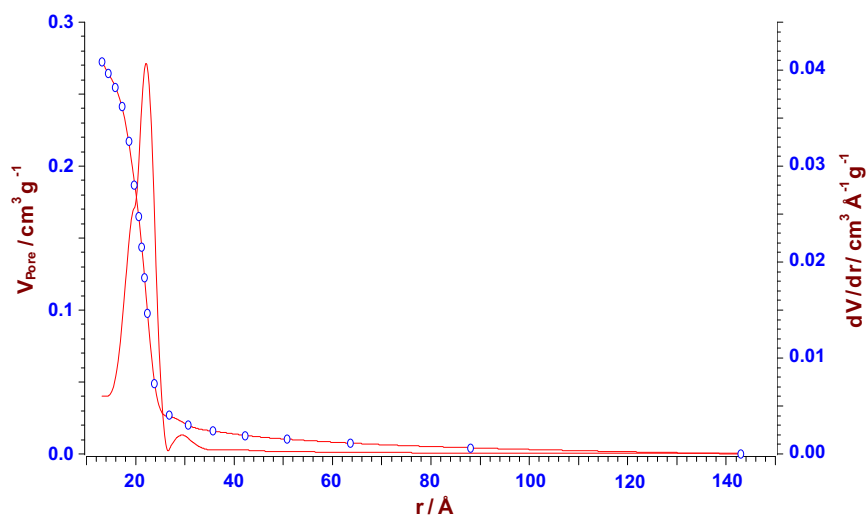


Figure 8 Pore distribution (B.J.H.) of  $\text{Al}_2\text{O}_3\text{-500}$ .

### 3.6. FESEM–EDX analysis

As can be seen from Fig. 9, the morphology of the boehmite precursor comprised mainly of wormhole-like structure without significant order of pore arrangement, which supports the observation in the BJH analysis. Addition of surfactant has little effect on the morphology of the synthesized mesoporous  $\gamma$ -alumina, the FESEM images of  $\text{Al}_2\text{O}_3\text{-PS-500}$  and  $\text{Al}_2\text{O}_3\text{-500}$  indicate that the  $\gamma$ -alumina retained the wormhole-like structure of the boehmite, however, there is an agglomeration of the particles in the  $\text{Al}_2\text{O}_3\text{-PS-500}$ , and the particles became flaky-like and appeared smaller than in the precursor and  $\text{Al}_2\text{O}_3\text{-500}$ , in agreement with the observation from the hysteresis loop. It is well known that the transformation from boehmite to  $\gamma$ -alumina is topotactic and, therefore,  $\gamma$ -alumina is likely to maintain the original morphology of the boehmite precursors (Liu et al., 2006). The inability of the addition of surfactant to change the morphology of the precursor can be connected to the fact that the interaction between the surfactant and boehmite is weak and cannot

destroy the hydrogen bonding interaction between boehmite layers that are formed by  $\text{O}^{2-}$  and  $\text{OH}^-$  of the  $\text{Al}^{3+}$  octahedral structure of the boehmite (Liu et al., 2008).

From the EDX spectra, only peaks of aluminium and oxygen can be observed. The EDX results showed that 100% alumina was obtained indicating very high purity of the synthesized alumina.

## 4. Conclusion

Mesoporous  $\gamma$ -alumina with relatively large surface area of  $222.7 \text{ m}^2/\text{g}$ , narrow pore size distribution centred at  $5.6 \text{ nm}$  and pore volume of  $0.45 \text{ cm}^3/\text{g}$  has been successfully synthesized from Kano kaolin in the presence of polyoxyethylene (40) stearate. Although mesoporous alumina was also obtained even in the absence of surfactant, the addition of the surfactant improved both the textural properties and the morphology of the synthesized mesoporous gamma alumina. The surface area, pore size distribution and pore volume were

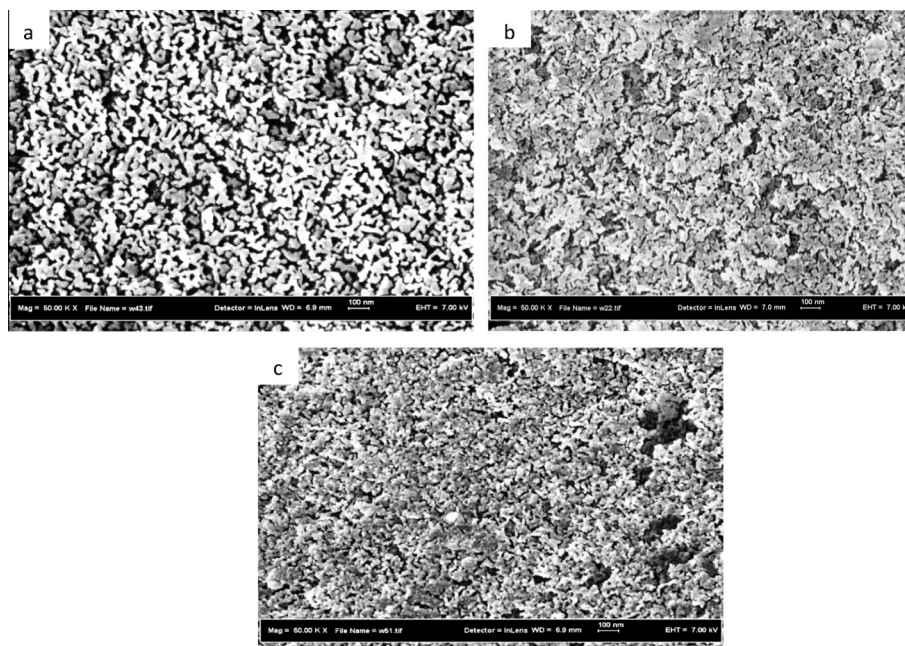


**Figure 9** FESEM images of (a) precursor, (b)  $\text{Al}_2\text{O}_3$ -PS-500 and (c)  $\text{Al}_2\text{O}_3$ -500.

found to be higher in the alumina synthesized in the presence of PS. Furthermore, the average crystallite size was calculated to be 3.33 nm for  $\text{Al}_2\text{O}_3$ -PS-500 as against 2.68 nm for  $\text{Al}_2\text{O}_3$ -500. The interaction between PS and precursor was found to be weak as a result it can easily be removed from the precursor after calcination, and the result showed a clear advantage of using PS as a surfactant as it would lead to a synthesis of mesoporous alumina with high thermal stability as indicated by the TG-DTA result. Mesoporous alumina with high thermal stability and narrow pore-size distribution is a potential material in adsorptive and catalytic applications.

#### Acknowledgements

The authors would like to acknowledge the Research Management Centre (RMC), UTM and the management of Sa'adatu Rimi college of education Kumbotso, Kano state, Nigeria for the financial support provided.

#### References

- Afroz, F.B., Tafreshi, M.J., 2014. Synthesis of  $\gamma$ - $\text{Al}_2\text{O}_3$  nano particles by different combustion modes using ammonium carbonate. *Indian J. Pure Appl. Phys.* 52, 378–385.
- Awual, R., Hasan, M., 2014. A novel fine-tuning mesoporous adsorbent for simultaneous lead (II) detection and removal from wastewater. *Sens. Actuators B* 202, 395–403.
- Darban, A.K., Kianinia, Y., Taheri-nassaj, E., 2013. Synthesis of nano-alumina powder from impure kaolin and its application for arsenite removal from aqueous solutions. *J. Environ. Health Sci. Eng.* 11 (1), 1–11.
- Du, C., Yang, H., 2012. Investigation of the physicochemical aspects from natural kaolin to Al-MCM-41 mesoporous materials. *J. Colloid Interface Sci.* 369 (1), 216–222.
- Eze, K.A., Nwadiodbu, J.O., Nwankwere, E.T., 2012. Effect of acid treatment on the physicochemical properties of kaolin clay. *Arch. Appl. Sci. Res.* 4 (2), 792–794.
- Feng, L., Zhang, H., Mao, P., Wang, Y., Ge, Y., 2011. Superhydrophobic alumina surface based on stearic acid modification. *Appl. Surf. Sci.* 257, 3959–3963.
- Ghosh, S., Bose, P., Basak, S., Naskar, M.K., 2015. Solvothermal-assisted evaporation-induced self-assembly process for significant improvement in the textural properties of  $\gamma$ - $\text{Al}_2\text{O}_3$ , and study dye adsorption efficiency. *J. Asian Ceram. Soc.* (accepted 1702.15).
- Jiang, X., Suzuki, N., Bastakoti, B.P., Wu, K.C.-W., Yamauchi, Y., 2012. Synthesis of continuous mesoporous alumina films with large-sized cage-type mesopores by using diblock copolymer. *Chem. Asian J.* 7 (7), 1713–1718.
- Jiao, W.Q., Yue, M.B., Wang, Y.M., He, M.-Y., 2012. Synthesis of morphology-controlled mesoporous transition aluminas derived from the decomposition of alumina hydrates. *Micropor. Mesopor. Mater.* 147, 167–177.
- Kang, M., Kin, D., Hwan, S., Uk, J., Eui, J., Man, Ji., 2004. Preparation of stable mesoporous inorganic oxides via nano-replication technique. *Catal. Today* 95, 695–699.
- Khalil, K.M.S., 2008. Formation of mesoporous alumina via hydrolysis of modified aluminum isopropoxide in presence of CTAB cationic surfactant. *Appl. Surf. Sci.* 255, 2874–2878.
- Lesaint, C., Kleppa, G., Arla, D., Wilhelm, R.G., Gisle, Ø., 2009. Synthesis and characterization of mesoporous alumina materials with large pore size prepared by a double hydrolysis route. *Micropor. Mesopor. Mater.* 119 (1–3), 245–251.
- Liu, Q., Wang, A., Wang, X., Zhang, T., 2006. Mesoporous  $\gamma$ -alumina synthesized by hydro-carboxylic acid as structure-directing agent. *Micropor. Mesopor. Mater.* 92, 10–21.
- Liu, Q., Wang, X., Gao, P., Wang, X., Zhang, T., 2008. Synthesis, characterization and catalytic applications of mesoporous  $\gamma$ -alumina from boehmite sol. *Micropor. Mesopor. Mater.* 111, 323–333.
- Márquez-Alvarez, C., Žilková, N., Jaouin, P.-P., Čejka, J., 2008. Synthesis, characterization and catalytic applications of organized mesoporous aluminas. *Catal. Rev.* 50 (2), 222–286.
- Mohsen, Q., El-maghraby, A., 2010. Characterization and assessment of Saudi clays raw material at different area. *Arab. J. Chem.* 3, 271–277.

- Naik, B., Ghosh, N.N., 2009. A review on chemical methodologies for preparation of mesoporous silica and alumina based materials. *Recent Pat. Nanotechnol.* 3 (3), 213–24.
- Oveisi, H., Rahighi, S., Jiang, X., Nemoto, Y., Beitollahi, A., Wakatsuki, S., Yamauchi, Y., 2010. Unusual antibacterial properties of mesoporous titania films: drastic improvement by controlling surface area and crystallinity. *Chem. Asian J.* 5 (9), 1978–1983.
- Pan, F., Lu, X., Wang, T., Wang, Y., Zhang, Z., Yan, Y., Yang, S., 2013. Synthesis of large-mesoporous  $\gamma$ - $\text{Al}_2\text{O}_3$  from coal-series kaolin at room temperature. *Mater. Lett.* 91 (1), 136–138.
- Polarz, S., 2004. Ordered mesoporous materials. *Encyclopedia Nanosci. Technol.* 8, 239–258.
- Rangel-Porras, G., Rangel-Rivera, P., Ramos-Ramirez, E., 2015. Changes in the thermal behavior and surface area of transitional alumina induced by the inclusion of metallic ions. *Synthesis React. Inorg. Met. Org. Nano-Met. Chem.* 45 (5), 629–638.
- Samadhi, T.W., Lismana, K.R., Fuadi, K., 2011. Synthesis of  $\gamma$ - $\text{Al}_2\text{O}_3$  catalyst support from kaolin of Indonesian origin. *J. Eng. Sci.* 43 (2), 113–126.
- Sapniwat, S., Pavarajarn, V., Kangwansupamonkon, W., Soottitantawat, A., 2013. Synthesis of porous  $\gamma$ -alumina assisted by resorcinol-formaldehyde gel. *Chiang Mai J. Sci.* 40 (6), 1006–1012.
- Shi, X., Yang, C., Zhang, L., Lu, Z., Zhu, Y., Tang, D., Cui, C., Zeng, H., 2014. Mesoporous alumina microfibres in situ transformation from AACH fibres and the adsorption performance. *J. Nanomater.* 2014, 1–6.
- Xue, W., Zhou, Y.C., Song, B.A., Shi, X., Wang, J., Yin, S.T., Hu, D.Y., Jin, L.H., Yang, S., 2009. Synthesis of biodiesel from *Jatropha curcas* L. seed oil using artificial zeolites loaded with  $\text{CH}_3\text{COOK}$  as a heterogeneous catalyst. *Nat. Sci.* 1, 55–62.
- Yang, H., Liu, M., Ouyang, J., 2010. Novel synthesis and characterization of nanosized  $\gamma$ - $\text{Al}_2\text{O}_3$  from kaolin. *Appl. Clay Sci.* 47 (3–4), 438–443.
- Yue, M.B., Xue, T., Jiao, W.Q., Wang, Y.M., He, M.Y., 2011. CTAB-directed synthesis of mesoporous  $\gamma$ -alumina promoted by hydroxy carboxylate: the interplay of tartrate and CTAB. *Solid State Sci.* 13, 409–416.
- Zhu, S., Huang, R., Hong, M., Jiang, Y., Hu, Z., Liu, C., Pei, Y., 2009a. Effects of polyoxyethylene (40) stearate on the activity of P-glycoprotein and cytochrome P450. *Eur. J. Pharm. Sci.* 37, 573–580.
- Zhu, Z., Liu, H., Sun, H., Yang, D., 2009b. Surfactant assisted hydrothermal and thermal decomposition synthesis of alumina microfibres with mesoporous structure. *Chem. Eng. J.* 155, 925–930.